# Anthropogenic carbon changes in the Irminger Basin (1981-2006): Coupling $\delta^{13}C_{DIC}$ and DIC observations

Racapé, V.[a*], Pierre C.[a], Metzl, N.[a*], Lo Monaco, C.[a], Reverdin, G.[a], Olsen, A. [b,c], Morin, P.[d], Vazquez-Rodriguez, M.[e], Rios, A.F.[f] and Perez, F.F.[f]

[a]*LOCEAN-IPSL, Université Pierre et Marie Curie, Case 100, 4 place Jussieu, Paris, 75252 Cedex 05, France*

[b]*Institute of Marine Research, P.O. Box 1870 Nordnes, 5817 Bergen, Norway*

[c]*Uni Bjerknes Centre, Allégaten 55, N-5007 Bergen, Norway*

[d] *Chimie Marine, UMR 7144 CNRS & UPMC, Station Biologique, B.P. 74, 29682 Roscoff, France*

[e] *Oceanography Department - SOEST, University of Hawaii at Manoa, 1000 Pope Rd. Honolulu, HI 96822, Hawaii*

[f]*Instituto de Investigaciones Marinas, CSIC, Eduardo Cabello 6, 36208 Vigo, Spain*

* Corresponding Author:

Racapé Virginie: vrlod@locean-ipsl.upmc.fr

Phone: 00 33 (0)1 44 27 48 61 - Fax: 00 33 (0)1 44 27 49 93

## Abstract

The North Atlantic subpolar gyre is considered to be one of the strongest marine anthropogenic $CO_2$ sinks, a consequence of extensive deep convection occurring during winter. Observations collected in this region since 1981 have shown large changes in Dissolved Inorganic Carbon (DIC) concentrations in intermediate and deep waters, which have been attributed to both anthropogenic $CO_2$ penetration and natural variability in the ocean carbon cycle (Wanninkhof et al., 2010). In this context, we describe new $\delta^{13}C_{DIC}$ observations obtained in the Irminger Basin during two OVIDE cruises (2002 and 2006) which we compare to historical data (TTO-NAS 1981) in order to estimate the oceanic $^{13}C$ Suess Effect over the more than twenty years that separates these surveys. The data reveal a significant decrease in $\delta^{13}C_{DIC}$, of between -0.3 ‰ and -0.4 ‰ from 1981 to 2006. The anthropogenic change, extracted by using the extended Multi Linear Regression (eMLR) approach, explains 75% of this signal for oldest water mass and 90% for youngest. The reminding signal is due to the natural processes, such as remineralization and vertical mixing. The eMLR method was also applied to DIC measurements which i) reveal strong relationships between the increase of anthropogenic $CO_2$ and the oceanic $^{13}C$ Suess Effect over the whole water column during the 25-year period and ii) support the hypothesis of change in the $C_{ant}$ storage rate in the Irminger basin between 1981 and 2006.



*Keywords: Oceanic $^{13}C$ Suess effect, anthropogenic carbon, North Atlantic Ocean, Decadal variation*


## 1. Introduction

Carbon dioxide ($CO_2$) emissions from fossil fuel burning and land use change have increased strongly in recent years, from 5.5 PgC $yr^{-1}$ (Pg = $10^{15}$ g) in 1970 to 8.4 PgC $yr^{-1}$ in 2000 (Raupach et al., 2007) and 9.9 PgC $yr^{-1}$ in 2006 (Canadell et al., 2007). The consequence of this human-induced perturbation is the accumulation of anthropogenic $CO_2$ in the atmosphere, which reached the benchmark of 100 ppm in 2007 (Le Quéré et al., 2009), and is the most significant driver of the increased greenhouse effect (IPCC, 2007). The modification of the isotopic composition of the atmospheric $CO_2$, known as the $^{13}C$ Suess Effect, provides key evidence for the fossil source of this carbon. The anthropogenic $CO_2$ is produced by combustion of fossil fuels, which are biologically sourced and strongly depleted in $^{13}C$ relatively to $^{12}C$ (Tans, 1981; Andres et al., 1996), thus decreasing the $^{13}C/^{12}C$ ratio of atmospheric $CO_2$ ($\delta^{13}C_{CO2}$). Based on atmospheric measurements sampled at different SIO-stations (Scripps Institution of Oceanography, http://cdiac.ornl.gov/trends/co2/iso-sio/iso-sio.html), the $^{13}C$ Suess Effect was evaluated to be ~ -0.024 ‰ $yr^{-1}$ since the 1980's. Isotopic exchange since the Industrial Revolution has caused the $^{13}C/^{12}C$ ratio of dissolved inorganic carbon ($\delta^{13}C_{DIC}$) in sea water to decrease substantially (Kroopnick, 1985; Broecker and Maier-Reimer, 1992; Gruber et al., 1999; Sonnerup et al., 2000; McNeil et al., 2001; Quay et al., 2003, 2007; Olsen et al., 2006; Tagliabue and Bopp, 2008; Olsen and Ninnemann, 2010; Racapé et al., 2010). This $^{13}C$ decrease, known as the

oceanic $^{13}C$ Suess Effect, provides additional information allowing us to further understand mechanism of ocean $C_{ant}$ uptake in various ocean regions (e.g. McNeil et al. 2001; Olsen et al., 2006, Quay et al., 2007.)

As much as 23% of the total oceanic $C_{ant}$ inventory of 106±17 PgC is stored in the North Atlantic Ocean (Sabine et al., 2004). This is mainly due to the large deep convection process during winter which quickly moves anthropogenic $CO_2$ away from the surface waters of the Labrador, Irminger and Greenland Seas into the large underlying ocean volume deep ocean, thus maintaining their anthropogenic $CO_2$ uptake capacity, combined with the extensive transport of anthropogenic $CO_2$ into these region from further South (Alvarez et al 2003; Jeansson et al., 2011, Gruber et al., 2009) as well as from the atmosphere (Gruber et al., 2009).The Irminger basin contributes strongly to the $C_{ant}$ storage in the North Atlantic Ocean, but ocean $CO_2$ observations conducted in this region since 1981 have shown large variations in anthropogenic DIC concentrations in subsurface waters as well as in intermediate and deep waters (Perez et al., 2008, 2010). These authors suggested that the $C_{ant}$ storage rate in this region has not been steady since the mid-nineties and suggest that the Labrador Sea Water (LSW) contribution to the storage of $C_{ant}$ in the Irminger basin has been reduced from 66% in 1990's to 49% in 2000's coherent with a decreasing rate of air-sea $CO_2$ fluxes observed in the same region (e.g. Corbière et al., 2007; Metzl et al., 2010). This signal is likely associated to the large-scale climatic forcing provided by the shift in the North Atlantic Oscillation (NAO) in 1995-96 and posed the problem of separating the anthropogenic signal from the natural variability (Wanninkhof et al., 2010).

To further understand the anthropogenic component of the carbon system changes in the Irminger Basin, we investigate the coupling between changes in DIC and $\delta^{13}C_{DIC}$. In this analysis, we first describe the $\delta^{13}C_{DIC}$ observations obtained in this region during the OVIDE cruises carried out in 2002 and 2006. Then we evaluate jointly the oceanic $^{13}C$ Suess Effect and $C_{ant}$ accumulation by comparing the OVIDE data to historical data sampled in 1981 (TTO-NAS) in deep water masses, LSW, North East Atlantic Deep Water (NEADW) and Denmark Strait Overflow Water (DSOW). As the $\delta^{13}C_{DIC}$ and DIC anthropogenic signals may be masked by changes in biological activity and/or ocean dynamics, we used an extended Multi Linear Regression (eMLR) approach to remove natural variability.

# 2. Data Collection

## 2.1. **OVIDE dataset**

The OVIDE project contributes to the observations of both circulation and water mass properties along a section from Greenland to Portugal. Here we focus on the observations collected in the Irminger Basin between 42.5°W and 30°W in June 2002 and June 2006 (Fig.1a). Continuous measurements of temperature, salinity and dissolved oxygen concentration were performed in the Irminger Basin at

twenty CTD-$O_2$ stations (Conductivity-Temperature-Depth-Oxygen). Sea water samples were also collected at different depths to determine the concentration of nutrients and anthropogenic tracers, such as $\delta^{13}C_{DIC}$, DIC and CFCs as well as the dissolved oxygen concentration and salinity for sensor calibration. Except for the $\delta^{13}C_{DIC}$, the measurements methods have been described previously (Lherminier et al., 2007; Perez et al., 2008, 2010; OVIDE web site http://www.ifremer.fr/lpo/ovide/). The sea-water samples for $\delta^{13}C_{DIC}$ were collected in 125ml glass bottles at selected stations, chosen to cover the Irminger Basin as a whole. All samples were poisoned with $HgCl_2$ (1ml of saturated solution) before storage in a dark environment, and analysis in the LOCEAN/IPSL laboratory. The DIC was extracted from the seawater by acidification with phosphoric acid ($H_3PO_4$ 85%) and $CO_2$ gas that was produced was collected in a vacuum system following the procedure described by Kroopnick (1974). The isotopic composition of $CO_2$ was determined using a dual inlet-isotopic ratio mass spectrometer (SIRA9-VG) by comparing the $^{13}C/^{12}C$ ratio of the sample (R) to the $^{13}C/^{12}C$ ratio of a reference material (R*), the Vienna-Pee Dee Belemnite (V-PDB). The isotopic composition is expressed in the δ-unit defined by Craig (1957), as follows (equation 1):

$$\delta^{13}C_{DIC} \text{ (‰ vs V-PDB)} = [(R/R^*) - 1] \times 1000 \quad (1)$$

The precision and the reproducibility of this method are close to ± 0.01 ‰ and 0.02 ‰, respectively (Vangriesheim et al., 2009; Racapé et al., 2010).

## 2.2. **TTO-NAS dataset**

The Transient Tracers in the Ocean (TTO) cruises were conducted from April to October of 1981 in the North Atlantic Ocean (Brewer et al., 1986). The Irminger Basin was covered during legs 5 and 6 in August 1981 (Fig.1a). In this study, we use the data obtained at stations 175 through 183 (leg 6) and 167 (leg 5). Following Holliday et al. (2006; Fig.1a) and θ-S characteristics, water masses observed at station 167 were consistent with those observed at the OVIDE stations located in the East Greenland Current. The TTO-NAS dataset considered in this work and instrumental techniques were obtained from the Carbon Dioxide Information Analysis Center (CDIAC, http://mercury.ornl.gov/cdiac/). During TTO, $\delta^{13}C_{DIC}$ was measured by the Carbon Dioxide Research Group at Scripps Institute of Oceanography with a method described by Gruber et al. (1999) and comparable to the one used for the OVIDE data. All values flagged as suspicious in the original data set were discarded, as well as data points where the replicate analyses differed by more than 0.12 ‰. The overall precision for these data is 0.04 ‰ (Gruber et al., 1999).

We can notice that no Certified Referenced Material (CRM) for the carbon parameters was available at the time the TTO-NAS was carried out. To elucidate any bias in these data, Tanhua and Wallace (2005) carried out a cross-over analysis between TTO data set and overlapping modern cruises referenced to CRMs. Based on this analysis, they found that the TTO data are biased high and recommend an adjustment of -3.6 µmol $kg^{-1}$ for Total Alkalinity ($A_T$) and -2.4 µmol $kg^{-1}$ for DIC

calculated from corrected $A_T$, $pCO_2$ and modern carbon system constants. These adjustments were applied to our data set.

# 3. Results

## 3.1. Recent $\delta^{13}C_{DIC}$ observations in the Irminger Basin (2002 and 2006)

Figure 2 shows the $\delta^{13}C_{DIC}$ distribution in the water column between the East Greenland coast (42.5°W) and the Reykjanes Ridge (30°W) obtained during the OVIDE cruises conducted in 2002 and 2006. The $\delta^{13}C_{DIC}$ data in 2002 deviate slightly from those observed in 2006 with the latter being a bit lower. The highest $\delta^{13}C_{DIC}$ observations (>1 ‰) are detected in the surface waters of the Irminger basin, predominantly close to the Greenland coast (~1.5 ‰), while the lowest $\delta^{13}C_{DIC}$ values (0.4 ‰-0.5 ‰) were measured in 2006 in the upper 1000 m along the Greenland continental slope. Below 1200 m, the $\delta^{13}C_{DIC}$ distribution is quite homogeneous in the whole basin for both periods. In 2002, we also observed one low $\delta^{13}C_{DIC}$ value (0.49 ‰) in subsurface waters. This sample was collected at station 6, located at the eastern boundary of the East Greenland Coastal Current (EGCC, Lherminier et al., 2007). In the following we investigate the mechanisms that could explain these different ranges along the slope.

The Greenland continental slope is characterized by a particular hydrographic structure with the shallow layers (less than 1000 m) strongly influenced by the mixing between the cold and fresh Arctic waters transported by the East Greenland Current (EGC) and the warm and saline Atlantic waters carried southward by the Irminger Current retroflection (IC; Bacon et al., 2002; Sutherland and Pickart, 2008; Fig.1a).The front between the EGC and IC retroflection (Pickart et al., 2005) enhances biological activity in surface water (Holliday et al., 2009) and thus increases $\delta^{13}C_{DIC}$ values. West of the EGC, the EGCC flows southward advecting cold fresh waters loaded by glacier and sea ice melt from coastal runoff and arctic regions (Bacon et al., 2002). Louarn et al. (2009) have shown that this region was associated with a maximum in CFC-11 in 2006. OVIDE observations suggest that the minimal $\delta^{13}C_{DIC}$ values (0.4 ‰-0.5 ‰) in the Irminger Basin trace the Western Boundary Currents (WBC: EGC and EGCC). The polar origin of these WBC characterized by high CFC-11 concentration may explain these low values in $\delta^{13}C_{DIC}$ due to the enhanced atmospheric $CO_2$ uptake. This regional anomaly will not be included in the analysis of decadal changes.

## 3.2. The evolution of $\delta^{13}C_{DIC}$, DIC and $C_{ant}$ from 1981 to 2006

The $\delta^{13}C_{DIC}$ and dissolved inorganic carbon (DIC) distributions in the Irminger Basin in 1981, 2002 and 2006 are shown in Figure 3. A large decrease in $\delta^{13}C_{DIC}$ (0.3 ‰-0.4 ‰) is evident in the whole basin (Fig. 3a). This corresponds to our expectations given the Suess Effect but unlike to what is expected, no increase in DIC is observed in the water column between 1981 and 2006 (Fig. 3b). Interestingly, below 1500 m, the DIC appears to have decreased slightly since 1981 (<5 μmol $kg^{-1}$).

These observations suggest that the natural variability of the carbon cycle masks the signal expected from anthropogenic carbon uptake and storage in this region. In previous studies, Perez et al. (2008, 2010) have estimated the $C_{ant}$ concentrations in deep water masses in the Irminger Basin (u/cLSW, NEADW, DSOW; Fig.1b) and have highlighted an increase in anthropogenic carbon close to 10 µmol $kg^{-1}$ over the whole basin since 1981. Here we investigate the observed $\delta^{13}C$ changes versus anthropogenic $CO_2$ as determined by Perez et al. (2008, 2010) using the $\varphi C_T°$ method, a data-based diagnostic approach that use subsurface layer (100-200m) as water-mass properties reference (Vázquez-Rodríguez et al., 2009). The results (Fig. 4, Table 1) show clear relationships between the $\delta^{13}C$ changes and the anthropogenic $CO_2$ concentration for all deep water masses of the Irminger Basin. The largest changes ($\Delta C_{ant}$= 9.8 ± 1.7 µmol $kg^{-1}$, $\Delta\delta^{13}C_{DIC}$ = -0.38 ± 0.06 ‰) are observed in the uLSW, a young ventilated water mass formed mostly in the 2000's. The minimum change in $C_{ant}$ was recorded in the NEADW (8.9 ± 1.9 µmol $kg^{-1}$). For $\delta^{13}C_{DIC}$ we observed the smallest change (-0.27 ± 0.09 ‰) in cLSW. In addition, the results (Fig.4) show different relationships between $\delta^{13}C_{DIC}$ and the anthropogenic $CO_2$ concentration for the selected water masses over the 25-years period. Natural mechanisms can explain these differences, as these water masses have diverse histories, diverse imprints of vertical mixing or remineralization, and as the impact of gas exchange on $CO_2$ and $\delta^{13}C_{DIC}$ depends on the sea surface residence time. To estimate the anthropogenic effect on both $\delta^{13}C_{DIC}$ and DIC concentration, it is necessary to correct the observed signal for the natural variability.

## 3.3. Separating natural and anthropogenic signals

### 3.3.a. eMLR calculation

To extract the $\delta^{13}C_{DIC}$ and DIC anthropogenic signals, we used the extended Multi Linear Regression method which was first introduced by Sonnerup et al. (2000) and latter reviewed and formalized by Friis et al. (2005). Based on hydrological and biogeochemical parameters, two predictive equations are determined from a multi linear regression (Wallace, 1995). Using a selection of parameters that describe the underlying processes, these predictive equations have to adequately describe the spatial variability of $\delta^{13}C_{DIC}$ and DIC distributions. In our implementation we first included four parameters, potential temperature (θ, °C), Salinity (S), Silicate (Si, µmol $kg^{-1}$) and Total Alkalinity ($A_T$, µmol $kg^{-1}$) in the predictive equations. Then we evaluated the suitability of a fifth parameter (X in Equations 2, 3: phosphate ($PO_4^{3-}$), nitrate ($NO_3^-$) or AOU). As two predictive equations are determined from two independent datasets sampled in the same location during different years (1981 and 2006), the propagation of independent parameter measurement errors is reduced. These two equations are applied on one or the other dataset and the differences in the predictive DIC and $\delta^{13}C_{DIC}$ values reveal the anthropogenic change. The net eMLR equations are expressed as:

$$\Delta DIC^{eMLR} = (a_3-a_1)\theta + (b_3-b_1)S + (c_3-c_1)Si + (d_3-d_1)A_T + (e_3-e_1)X + (k_3-k_1) \quad (2)$$

$$\Delta\delta^{13}C_{DIC}^{eMLR} = (a_4-a_2)\theta + (b_4-b_2)S + (c_4-c_2)Si + (d_4-d_2)A_T + (e_4-e_2)X + (k_4-k_2) \quad (3)$$

The significance of each term and of the MLR is estimated from a stepwise Multi Linear Regression. Except for AOU, statistical conditions listed by Ostrom (1990) are met for all predictive equations (i.e. AOU is no longer considered in this work).

The underlying natural correlation of DIC and $\delta^{13}C_{DIC}$ with the selected independent parameters must not change over the time period of interest. As a result, temporal evolution of the selected parameters must be expressed by regression coefficients and independent of the anthropogenic variability. The investigation on the predictive variables has shown a large decrease in alkalinity and in phosphate and an increase in nitrate over 25 years ($\Delta A_T \sim 10$ µmol kg$^{-1}$, $\Delta PO_4^{3-} \sim 0.15$µmol kg$^{-1}$ and $\Delta NO_3^- \sim 1$µmol kg$^{-1}$; Fig. 5). These differences are not clearly explained although the evolution of the different nutrients (Figs.5a and 5b) seems to be consistent in time. These could be related either to analytical errors or natural variability.

Backward and forward calculations also revealed large differences with $PO_4^{3-}$ as fifth parameter. As $PO_4^{3-}$ do not seem to produce a consistent pattern for both DIC and $\delta^{13}C_{DIC}$ changes, only those obtained with $NO_3^-$ as fifth predictive variable are discussed in this paper. Regression coefficients and statistics for predictive DIC and $\delta^{13}C_{DIC}$ are summarized in table 2.

### 3.3.b. Coupling $\delta^{13}C_{DIC}$ and DIC anthropogenic signals

The anthropogenic changes in $\delta^{13}C_{DIC}$ and DIC estimated by the eMLR method from 1981 to 2006 in the Irminger Basin are displayed in figures 6 and 7 (region 41.4°W- 34°W / 60°N- 59°N , these boundaries were established based on $\delta^{13}C_{DIC}$ data available in 1981). As no systematic difference is observed between the backward and forward calculations (Fig. 6), we focus this work on the results obtained from eMLR applied on the OVIDE dataset for a better coverage (Table 2: fits #3-#1 for $\Delta DIC^{eMLR}$ and fits #4-#2 for $\Delta\delta^{13}C_{DIC}^{eMLR}$).

We first recall that more negative values of $\Delta\delta^{13}C_{DIC}^{eMLR}$ indicate the strongest oceanic $^{13}C$ Suess Effect. In general, $\Delta\delta^{13}C_{DIC}^{eMLR}$ is less negative than observed $\Delta\delta^{13}C_{DIC}$ (Table 1), indicating that the oceanic $^{13}C$ Suess Effect is amplified by natural processes such as remineralization which intensifies this signal (reduce $\delta^{13}C_{DIC}$). The general pattern (Fig. 6) shows a strong relationship between the increase in the oceanic $^{13}C$ Suess Effect and the anthropogenic carbon change in all water masses: the youngest water masses, uLSW and DSOW (Rhein et al., 2002; Louarn et al., 2009) are characterized by the strongest oceanic $^{13}C$ Suess Effect (-0.35 to -0.4 ‰) and the highest anthropogenic carbon change (6 to10 µmol kg$^{-1}$). In the oldest water mass, NEADW, we observed low anthropogenic carbon changes (<2 µmol kg$^{-1}$), but significant $\Delta\delta^{13}C_{DIC}^{eMLR}$ change (>-0.30 ‰) suggesting a real anthropogenic signature.

## 4. Discussion

In all water masses, we observe a decline in $\delta^{13}C_{DIC}$ and $\Delta\delta^{13}C_{DIC}^{eMLR}$ reflecting the penetration of anthropogenic $CO_2$ (Figs. 3, 4, 6 and 7; Table 1). Indeed, the LSWs formed by deep winter convection in the Labrador Sea at the beginning of the 1990's (cLSW) and the 2000's (uLSW; Yashayaev et al., 2008), held 41% of the anthropogenic carbon stored in the Irminger Basin in 2006 (Perez et al., 2008). The Suess Effect is also large in these water masses with a time rate of change between -0.014 ‰ $yr^{-1}$ and -0.015 ‰ $yr^{-1}$. This is consistent with Quay et al. (2007) and Sonnerup and Quay (2012) who evaluated the Suess Effect in the subpolar region at -0.017 ± 0.005 ‰ $yr^{-1}$ (period: 1993-2003) and in the Labrador Basin at -0.014 ‰ $yr^{-1}$ (period: 1970-1995) respectively. In the atmosphere, $\delta^{13}C_{CO2}$ was reduced by ~0.027 ‰ $yr^{-1}$ between 1962 and 2003 (Francey et al., 1999; Olsen et al., 2006). The $\delta^{13}C_{DIC}$ in the Labrador Sea surface water is not in isotopic equilibrium with the atmospheric $\delta^{13}C_{CO2}$ because the residence time of the surface water is shorter than the time needed for $CO_2$ to reach isotopic equilibrium with the atmosphere (~10yr, Broecker and Peng, 1974; Lynch-Stieglitz et al., 1995). The cLSW have mostly not formed since 1997 (Lazier et al., 2002) and were thus no more in contact with the atmosphere. This is supported by the decline of CFC-12 concentration observed in this water mass since this time (Kieke et al., 2007). Based on the time rate of change by -0.015 ‰ $yr^{-1}$ (like in the uLSW and close to Sonnerup and Quay, 2012), we should observe a decrease in $\delta^{13}C_{DIC}$ of ~0.26 ‰ over the 17 year-period (1998-1981) rather than ~0.35 ‰ for the period of 25 years (Fig. 6). The difference between these two values might be explained by diapycnal mixing processes between cLSW and the upper water (Kieke et al., 2007; Perez et al., 2008).

The residence time of sea surface waters (~1yr, Yashayaev et al., 2008) is comparable to the time needed for $CO_2$ to reach equilibrium with the atmosphere. Based on the atmospheric $CO_2$ evolution between the 1980s and 2000s and using average sea surface conditions (T=5°C, S=35, $A_T$=2300 µmol $kg^{-1}$), the time rate of change in DIC in equilibrium with the atmospheric $CO_2$ was estimated to 0.72 µmol $kg^{-1}$ $yr^{-1}$. Considering this theoretical value and the complete renewal of the whole volumes of LSWs, we should observe an increase in DIC of 12 µmol $kg^{-1}$ (0.72 µmol $yr^{-1}$ x 17 years) and 18 µmol $kg^{-1}$ (0.72 µmol $yr^{-1}$ x 25 years) in the classical and upper LSW respectively (Fig. 8). The $C_{ant}$ change estimated from eMLR (< 10 µmol $kg^{-1}$) is thus much less than the change expected by assuming air-sea equilibrium of $CO_2$. This suggests that the entire volumes of these water masses have not been completely ventilated over the 25 years supporting the hypothesis from Perez et al. (2008, 2010) who concluded that the $C_{ant}$ storage rate in this region was reduced since the mid-nineties.

Figures 6 to 8 also reveal further mixing processes between several water masses. The NEADW characterized by a large range in both DIC and $\delta^{13}C_{DIC}$ changes are indeed strongly influenced by the DSOW and the LSWs (Perez et al., 2008, 2010). To validate this hypothesis, the Suess Effect should

be estimated in the eastern Irminger Basin as well as in the Iceland Basin in order to better understand the signal observed in the NEADW. The DSOW is made up of different water masses originating from the Arctic and from the Atlantic, and then mixes with the LSW and NEADW in the Irminger basin (Tanhua et al., 2005). Waters of Arctic origin could contribute to the high $^{13}C$ Suess Effect in the DSOW due to the recent contact of these water masses with the atmosphere before convection to the Deep Ocean. Further interpretation of these changes in DSOW would require investigating the isotopic composition of the DSOW upstream from the Irminger basin to better understand the invasion of anthropogenic $CO_2$ in this water mass.

## 5. Summary and conclusion

In this study, we have described new $\delta^{13}C_{DIC}$ observations obtained in the Irminger Basin during the summer 2002 and 2006 (OVIDE cruises). The homogeneous distribution of $\delta^{13}C_{DIC}$ was highlighted below 1200 m in the whole basin. Low $\delta^{13}C_{DIC}$ values (0.4 ‰-0.5 ‰) observed close to the Greenland coast in the upper 1000 m are likely associated to the EGCC. To estimate the anthropogenic carbon changes and the oceanic $^{13}C$ Suess effect, we compared this recent data set to historical data sampled in 1981 in this region (TTO-NAS cruises). The anthropogenic signal in both $\delta^{13}C_{DIC}$ and DIC measurements was isolated by using an extended Multi Linear Regression approach. There was a significant gap between the observed $\Delta\delta^{13}C_{DIC}$ and the calculated $^{13}C$ Suess Effect (Table 1). The same applied to DIC, suggesting that natural variations in the Irminger Sea have been of similar importance as the anthropogenic imprint over the last 25 years. Our results further showed strong relationships between the increase of anthropogenic $CO_2$ and the oceanic $^{13}C$ Suess Effect in the Irminger basin over the 25-years period. The anthropogenic change explains 75% of the observed $\delta^{13}C_{DIC}$ decrease for the oldest water mass and 90% for the youngest. The remaining part would be due to the natural processes of remineralization and diapycnal mixing between cLSW and uLSW and between DSOW, NEADW and LSWs. In addition, our results confirm a reduction of the $C_{ant}$ storage rate in this region between 1981 and 2006 (Perez et al., 2008; 2010). This work highlights the potential of coupling $\delta^{13}C_{DIC}$ and DIC observations to better separate natural or climate induced mechanisms and ocean uptake of anthropogenic $CO_2$. We strongly support to maintain such observations in the future and encourage new modeling experiments, including the oceanic $^{13}C$ system (Tagliabue and Bopp, 2008), to investigate the observed relationships between anthropogenic $CO_2$ and the oceanic $^{13}C$ Suess Effect.

**References**


Andres, R. J., Maxland, G., Bischoff, S., 1996. Global and latitudinal estimates of $\delta^{13}C$ from fossil fuel consumption and cement manufacture. Carbon Dioxide Information Analysis Center, CDIAC Communications, 22, Oak Ridge Natl. Lab, Oak Ridge, Tenn.

Alvarez. M, Rios, A. F., Perez, F. F., Bryden, H. L., Roson, G., 2003. Transports and budgets of total inorganic carbon in the subpolar and temperate North Atlantic. Global Biogeochem. Cycles 17, 1002, doi: 10.1029/2002GB001881.

Bacon, S., Reverdin, G., Rigor, I. G., Snaith, H. M., 2002. A freshwater jet on the east Greenland shelf. J. Geoph. Res. 107 (C7), 3068. doi: 10.1029/2001JC000935.

Brewer, P.G., Takahashi, T., Williams, R.T., 1986. Transient traces in the ocean – Hydrography data and carbon dioxide systems with revised carbon chemistry data. NDP- 004/R1, Carbon Dioxide Information Analysis Center, Oak Ridge Natl. Lab, Oak Ridge, Tenn.

Broecker, W. S. and Peng, T.H., 1974. Gas exchange rates between air and sea. Tellus 26, 21-35.

Broecker, W.S. and Maier-Reimer, E., 1992. The influence of air and sea exchange on the carbon isotope distribution in the sea. Global Biogeochem. Cycles 6 (3), 315-320.

Canadell, J.G., Le Quéré, C., Raupach, M.R.., Field, C.B., Buitehuis, E.T., Ciais, P., Conway, I.J., Gillett, N.P., Houghton, R.A., Marland, G., 2007. Contributions to accelerating atmospheric $CO_2$ growth from economic activity, carbon intensity, and efficiency of natural sinks. Proceedings of the National Academy of Sciences, USA 104, 18866-18870.

Corbière, A., Metzl, N., Reverdin, G., Brunet, C., Takahashi, T., 2007. Interannual and decadal variability of the oceanic carbon sink in the North Atlantic SubPolar Gyre. Tellus B 59 (2), 168-178. doi: 10.1111/j.1600-0889.2006.00232.x.

Craig, H., 1957. Isotopic standards for carbon and oxygen and correction factor for mass-spectrometric analysis of carbon dioxide. Geochim. Cosmochim. Acta 12, 133-149.

Francey, R. J., Allison, C. E., Etheridge, D. M., Trudinger, C. M., Enting, I. G., Leuenberger, M., Langefelds, R. L., Michel, E., Steele, L. P., 1999. A 1000-year high precision record of $\delta^{13}C$ in atmospheric $CO_2$. Tellus B 51, 170– 193.

Friis, K., Kortzinger, A., Patsch, J., Wallace, D., 2005. On the temporal increase of anthropogenic $CO_2$ in the subpolar North Atlantic. Deep-Sea Res. I 52 (5), 681-698. doi: 10.1016/j.dsr.2004.11.017.

Gruber, N., Keeling, C. D., Bacastow, R. B., Guenther, P. R., Lueker, T. J., Whalen, M., Meijer, H. A. J., Mook, W. G., Stocker, T. F., 1999. Spatiotemporal patterns of carbon-13 in the global surface oceans and the oceanic Suess effect. Global Biogeochem. Cycles 13 (2), 307-335.

Gruber, N., Gloor, M., Mikaloff Fletcher, S. E., Doney, S. C., Dutkiewicz, S. and co-authors, 2009. Oceanic sources, sinks, and transport of atmospheric $CO_2$. Global biogeochem. Cycles 23, GB1005. doi: 10.1029/2008GB003349.

Holliday, N., Waniek, J., Davidson, R., Wilson, D., Brown, L. and co-authors, 2006. Large-scale physical controls on phytoplankton growth in the Irminger Sea Part I: Hydrographic zones, mixing and stratification. J. Mar. Syst. 59 (3-4), 201-218. doi: 10.1016/j.jmarsys.2005.10.004.

Holliday, N. P., Bacon, S., Allen, J., McDonagh, E. L., 2009. Circulation and Transport in the estern Boundary Currents at Cape Farewell, Greenland. J. Phys. Oceanogr. 39 (8), 854-1870. doi: 10.1175/2009JPO4160.1.

IPCC, 2007. The physical science basis. In: Contribution of Working Group I to the Fourth assessment Report of the Intergouvernmental Panel on Climate Change (eds S. Solomon, D. Qin, M. Manning, Z. Chen, M. Marquis and co-authors), Cambridge University Press, Cambridge, United Kingdom and New York, NY, USA, p. 996

Jeansson, E., Olsen, A., Eldevik, T., Skjelvan, I., Omar, A. M., Lauvset, S., Nilsen, J. E. Ø., Bellerby, R. G. J., Johannessen, T., Falck, E., 2011. The Nordic Seas carbon budget: Sources, sinks and uncertainties. Global Biogeochem. Cycles 25, GB4010.

Kieke, D., Rhein, M., Stramma, L., Smethie, W. M., Bullister, J. L., Le Bel, D.A., 2007. Changes in the pool of Labrador Sea Water in the subpolar North Atlantic. Geophys. Res. Lett. 34 (6), 1-5. doi: 10.1029/2006GL028959.

Kroopnick, P., 1974. Correlations between $^{13}C$ and $\Sigma CO_2$ in surface waters and atmospheric $CO_2$. Earth Planet. Sci. Lett. 397-403.

Kroopnick, P., 1985. The distribution of $^{13}C$ of $\Sigma CO_2$ in the world oceans. Deep-Sea Res. 32(1), 57-84.

Lazier, J., Hendry, R., Clarke, R. A., Yashayaev, I., Rhines, P., 2002. Convection and restratification in the Labrador Sea, 1990–2000. Deep-Sea Res. 49, 1819–1835.

Le Quéré, C., Raupach, M.R., Canadell, J.G., Marland, G., Bopp, L. and co-authors, 2009. Trends in the sources and sinks of carbon dioxide. Nature Geosci. 2. doi:10.1038/ngeo689.

Lherminier, P., Mercier, H., Gourcuff, C., Alvarez, M., Bacon, S., Kermabon, C., 2007. Transports across the 2002 Greenland-Portugal Ovide section and comparison with 1997. J. Geophys. Res. 112 (C7), 1-20. doi: 10.1029/2006JC003716.

Louarn, E., Mercier, H., Morin, P., De Boisseson, E., Bacon, S., 2009. Upper Labrador Sea Water in the Irminger Sea during a weak convection period (2002-2006). Ocean Sci. Discuss. 6, 2085-2113. www.ocean-sci-discuss.net/6/2085/2009

Lynch-Stieglitz, J., Stocker, T. F., Broecker, W. S., Fairbanks, R. G., 1995. The influence of air-sea exchange on the isotopic composition of oceanic carbon: Observations and modelling. Global Biogeochem. Cycles 9 (4) 653-665.

McNeil, B., Matear, R., Tilbrook, B., 2001. Does carbon 13 track anthropogenic $CO_2$ in Southern ocean. Global Biogeochem. Cycles. 15, 3, 597-613

Metzl, N., Corbière, A., Reverdin, G., Lenton, A., Takahashi, T., and co-authors, 2010. Recent acceleration of the sea surface f $CO_2$ growth rate in the North Atlantic SubPolar Gyre (1993–2008) revealed by winter observations. Global Biogeochem. Cycles 24 (4), 1-13. doi: 10.1029/2009GB003658.

Olsen, A., Omar, A. M., Bellerby, R. G. J., Johannessen, T., Ninnemann, U. and co-authors, 2006. Magnitude and origin of the anthropogenic $CO_2$ increase and Suess effect in the Nordic seas since 1981. Global Biogeochem. Cycles, 20, 1-12. doi: 10.1029/2005GB002669.

Olsen, A. and Ninnemann, U., 2010. Large $\delta^{13}C$ gradients in the Preindustrial North Atlantic Revealed. Science 330, 658-659. doi: 10.1126/science.1193769

Ostrom, C. W. Jr., 1990, Time Series Analysis, Regression Techniques, Second Edition: Quantitative Applications in the Social Sciences, v. 07-009: Newbury Park, Sage Publications.

Pérez, F. F., Vázquez-Rodríguez, M., Louarn, E. Padin, X. A., Mercier, H., Ríos, A. F., 2008. Temporal variability of the anthropogenic $CO_2$ storage in the Irminger Sea. Biogeosciences 5, 1669-1679. doi:10.5194/bg-5-1669-2008

Pérez, F. F., Vázquez-Rodríguez, M., Mercier, H., Velo, A., Lherminier, P., Ríos, A. F., 2010. Trends of anthropogenic $CO_2$ storage in North Atlantic water masses. Biogeosciences 7 (5), 1789-1807. doi: 10.5194/bg-7-1789-2010.

Pickart, R. S., Torres, D. J., Fratantoni, P. S., 2005. The East Greenland Spill Jet. J. Phys. Oceanogr. 35, 1037–1053

Quay, P., Sonnerup, R., Westby, T., Stutsman, J., McNichol, A., 2003. Changes in the $^{13}C/^{12}C$ of dissolved inorganic carbon in the ocean as a tracer of anthropogenic $CO_2$ uptake. Global Biogeochem. Cycles 17 (1), 1004. doi:10.1029/2001GB001817.

Quay, P., Sonnerup, R., Stutsman, J., Maurer, J., Körtzinger, A., Padin, X. A., Robinson, C., 2007. Anthropogenic $CO_2$ accumulation rates in the North Atlantic Ocean from changes in the $^{13}C/^{12}C$ of dissolved inorganic carbon. Global Biogeochem. Cycles 21 (1), 1-15. doi: 10.1029/2006GB002761.

Racapé, V., Lo Monaco, C., Metzl, N., Pierre, C., 2010. Summer and winter distribution of $\delta^{13}C_{DIC}$ in surface waters of the South Indian Ocean (20°S-60°S). Tellus B 62 (5), 660-673. doi: 10.1111/j.1600-0889.2010.00504.x

Raupach, M.R., Marland, G., Ciais, P., Le Quéré, C., Canadell, J.G., Kleppe, G., Field, C.B., 2007. Global and regional drivers of accelerating $CO_2$ emissions. Proceedings of the National Acadamy Sciences, USA 104 , 10288-10293.

Rhein, M., Fischer, J., Smethie Jr., W. M., Smythe-wright, D., Weiss, R. F., Mertens, C., Min, D. H., Fleischmann, U., Putzka, A., 2002. Labrador Sea water: pathways, CFC inventory, and formation rates. J. Phy. Oceanogr. 32, 648-665.

Sabine, C. L., Feely, R. A., Gruber, N., Key, R. M., Lee, K. and co-authors, 2004. The oceanic sink for anthropogenic $CO_2$. Science (New York, N.Y.), 305(5682), 367-71. doi: 10.1126/science.1097403.

Schlitzer, R., 2002. Ocean Data View, http://www.awi-bremerhaven.de/Geo/ODV

Sonnerup, R. E., Quay, P. D., McNichol, A. P., 2000. The Indian Ocean $^{13}C$ Suess effect. Global. Biogeochem. Cycles. 14 (3), 903-916.

Sonnerup, R. E. and Quay, P.D., 2012. $^{13}C$ constraints on ocean carbon cycle models. Global Biogeochem. Cycles 26, GB2014, doi:10.1029/2010GB003980.

Sutherland, D. A. and Pickart, R. A., 2008. The East Greenland Coastal Current: Structure, variability and forcing. Prog. Oceanogr. 78, 58–77.

Tagliabue, A. and Bopp, L., 2008. Towards understanding global variability in ocean carbon-13. Global Biogeochem. Cycles 22, GB1025, doi:10.1029/2007GB003037.

Tanhua, T., Olsson, K. A., Jeansson, E., 2005. Formation of Denmark Strait Overflow Water and its hydro-chemical composition. J. Mar. Syst. 57 (3-4), 264-288. doi: 10.1016/j.jmarsys.2005.05.003.

Tanhua, T. and Wallace, D. W. R., 2005. Consistency of TTO-NAS inorganic carbon data with modern measurements. Geophys. Res. Lett. 32 (14). doi: 10.1029/2005GL023248.

Tans, P. A., 1981. Compilation of bomb $^{14}C$ data for use in global carbon model calculation, i SCOPE 16: Carbon Cycle Modelling, edited by B. Bolin, pp. 131-137, John Wiley, New York.

Våge, K., Pickart, R.S., Sarafanov, A., Knutsen, J., Mercier, H., and co-authors, 2011. The Irminger gyre: Circulation, convection, and interannual variability. Deep–Sea Res. I. doi:10.1016/j.dsr.2011.03.001

Vangriesheim, A., Pierre, C., Aminot, A., Metzl, N., Baurand, F. and co-authors. 2009. The influence of Congo river discharges in the surface and deep layers of the Gulf of Guinea. Deep-Sea Res. II. doi:10.1016/j.dsr2.2009.04.002.

Vázquez-Rodríguez, M., Touratier, F., Lo Monaco, C., Waugh, D. W., Padin, X. A., Bellerby, R. G. J., Goyet, C., Metzl, N., Ríos, A. F., Pérez, F. F., 2009. Anthropogenic carbon distributions in the Atlantic Ocean: data-based estimates from the Arctic to the Antarctic. Biogeosciences 6, 439–451. doi:10.5194/bg-6-439-2009

Wallace, D.W.R., 1995. Monitoring global ocean carbon inventories. OOSDP Background Report No. 5, Texas A&M University, College Station, Texas, USA.

Wanninkhof, R., Doney, S. C., Bullister, J. L., Levine, N. M., Warner, M., Gruber, N., 2010. Detecting anthropogenic $CO_2$ changes in the interior Atlantic Ocean between 1989 and 2005. J. Geophys. Res. 115 (C11), 1-25. doi: 10.1029/2010JC006251.

Yashayaev, I., Holliday, N., Bersch, M., Van Aken, H. M., 2008. The history of the Labrador Sea Water: Production, Spreading, Transformation and Loss, in: Arctic-Subarctic Ocean Fluxes: defining the role of the Northern Seas in climate, edited by: Dickson, R. R., Meincke, J., and Rhines, P., Springer, The Netherlands, pp 569–612.

## Acknowledgments

The OVIDE project was and is still supported by French research institutions, IFREMER and CNRS/INSU, and by the EU FP6 project CARBOOCEAN (511176) and EU FP7 project CARBOCHANGE (264879). This study is also a contribution to the international IMBER / SOLAS projects. The $^{13}C$ analyses have been also supported by CNRS/INSU (LEFE/OCEANS-C13 project). We want to acknowledge Herle Mercier and colleagues for leading OVIDE and helping in the $^{13}C$ sampling. We thank A. Tagliabue and L. Bopp for fruitful discussions. We are also grateful to R. Wanninkhof and T. Johannessen for their constructive comments.

## Tables

Table 1: Summary of observed and estimated mean changes in $\delta^{13}C_{DIC}$ and anthropogenic $CO_2$ (± standard deviation) in 4 deep water masses in the Irminger Basin for the period 1981-2006. $\delta^{13}C_{DIC}{}^{OBS}$ and $C_{ant}{}^{P2010}$ are shown in figure 4; $\Delta\delta^{13}C_{DIC}{}^{eMLR}$ and $\Delta DIC^{eMLR}$ are shown in figure 6.

| | $\Delta\delta^{13}C_{DIC}{}^{OBS}$ (‰) | $\Delta\delta^{13}C_{DIC}{}^{eMLR}$ (‰) | $\Delta C_{ant}{}^{P2010}$ (µmol kg$^{-1}$) | $\Delta DIC^{eMLR}$ (µmol kg$^{-1}$) |
|---|---|---|---|---|
| **uLSW** | -0.38 ± 0.06 | -0.34 to -0.38 | 9.8 ± 1.7 | 6 to 10 |
| **cLSW** | -0.27 ± 0.09 | -0.30 to -0.35 | 9.2 ± 2.8 | 4 to 7 |
| **NEADW** | -0.32 ± 0.10 | -0.22 to -0.30 | 8.9 ± 1.9 | -1 to 5 |
| **DSOW** | -0.34 ± 0.09 | -0.34 to -0.40 | 9.7 ± 3.1 | 5 to 9 |

Table 2: Regression coefficients and statistics for predicted DIC and $\delta^{13}C_{DIC}$ where equations have a form $y = a\theta + bS + cSi + dA_T + eNO_3^- + k$; [θ: potential temperature (°C); S: salinity (PSU); Si: silicate concentration (µmol $kg^{-1}$); $A_T$ : total alkalinity (µmol $kg^{-1}$); $NO_3^-$: nitrate concentration (µmol $kg^{-1}$); rmse: root mean square error (µmol $kg^{-1}$); $r^2$: regression coefficient; n: number of data].

| | | **Θ** | **S** | **Si** | **$A_T$** | **$NO_3^-$** | | | | |
|---|---|---|---|---|---|---|---|---|---|---|
| **fit** | **relationship** | **a** | **b** | **c** | **d** | **d** | **k** | **$R^2$** | **rmse** | **n** |
| **#1** | 1981 DIC | 3.910 | 21.453 | 0.132 | 0.893 | 3.880 | 790.67 | 0.96 | 1.40 | 243 |
| **#2** | 1981 $\delta^{13}C_{DIC}$ | 0.005 | 0.059 | 0.005 | 0.0005 | 0.049 | 2.72 | 0.97 | 0.02 | 19 |
| **#3** | 2006 DIC | 3.827 | 13.116 | 1.847 | 0.996 | 4.494 | 278.73 | 0.85 | 1.61 | 257 |
| **#4** | 2006 $\delta^{13}C_{DIC}$ | 0.012 | 0.180 | 0.038 | 0.003 | 0.060 | 15.30 | 0.79 | 0.06 | 30 |

## Figure captions

Fig. 1: Pattern of the main a) circulation (Holliday et al. 2006) and b) water masses (Perez et al., 2008) in the Irminger Basin. The sea surface circulation is given by solid lines (NAC for North Atlantic Current, IC for Irminger Current and EGC for East Greenland Current). The mid-depth circulation is given by dot-dashed line (u/cLSW for upper/classical Labrador Sea Water). The deep circulation is given by dotted lines (ISOW for Iceland–Scotland Overflow Water which is modified by mixing with the LSW to formed NEADW, North East Atlantic Deep Water, and DSOW for Denmark Strait Overflow Water). The density (σθ) boundaries were established following Kieke et al. (2007) and Yashayaev et al. (2008). The sampling locations in the Irminger Basin are shown by orange lines and symbols: the OVIDE samples (2002 and 2006) are given by the full line whereas the TTO samples (1981) are given by the dashed line. The crosses show the two stations where $\delta^{13}C_{DIC}$ was collected during the TTO cruises while the OVIDE $\delta^{13}C_{DIC}$ measurements were regularly sampled in water column along the OVIDE transect.

Fig.2: Vertical distribution of $\delta^{13}C_{DIC}$ (‰ vs V-PDB) sampled between the East Greenland coast and 30°W during OVIDE cruises in 2002 (grey symbols) and 2006 (white symbols). 4 areas are distinguished according to the literature (Väge et al., 2005; Holliday et al., 2006): the Reykjanes ridges (diamonds), the Irminger Current (circles), the Center of the Irminger Sea (squares) and the Western Boundaries Current region (triangles).

Fig.3: Vertical profiles of a) $\delta^{13}C_{DIC}$ (‰ vs V-PDB) and b) Dissolved Inorganic Carbon (DIC, µmol $kg^{-1}$) sampled during TTO-NAS 1981 (blacks triangles), OVIDE 2002 (grey squares) and OVIDE 2006 (white circles) in the Irminger Basin, between 41.4°W and 30°W.

Fig.4: Mean $\delta^{13}C_{DIC}$ (‰ vs V-PDB) versus mean anthropogenic carbon ($C_{ant}$) concentration (µmol $kg^{-1}$) estimated by Perez et al. (2010) for 1981 (black triangles), 2002 (grey squares) and 2006 (white circles) for each water mass (dashed lines: from right to left, upper Labrador Sea Water (uLSW), classical Labrador Sea Water (cLSW), North East Atlantic Deep Water (NEADW) and Denmark Strait Overflow Water (DSOW)). Each value is fitted with its standard deviation.

Fig.5: Vertical profiles of a) Phosphate concentration ($PO_4^{3-}$, µmol $kg^{-1}$), b) Nitrate concentration ($NO_3^-$, µmol $kg^{-1}$) and c) Total Alkalinity ($A_T$, µmol $kg^{-1}$) sampled during TTO-NAS 1981 (black triangles), OVIDE 2002 (grey squares) and OVIDE 2006 (white circles) in the Irminger Basin between 41.4°W and 30°W.

Fig.6: Vertical distribution of $\Delta DIC^{eMLR}$ and $\Delta\delta^{13}C_{DIC}{}^{eMLR}$ in function of sigma0, estimated from equations 2 and 3 respectively and applied either on the TTO data set (black squares) or on the OVIDE 2006 data set (white squares). Grey dashed lines show water masses boundaries established following Kieke et al. (2007) and Yashayaev et al. (2008). u/cLSW: upper/classical Labrador Sea Water; NEADW: North East Atlantic Deep Water; DSOW: Denmark Strait Overflow Water.

Fig.7: Estimated anthropogenic $CO_2$ increase ($\Delta DIC^{eMLR}$, µmol $kg^{-1}$) and anthropogenic $\delta^{13}C_{DIC}$ decrease ($\Delta\delta^{13}C_{DIC}{}^{eMLR}$, ‰) from 1981 to 2006 in the Irminger Basin along a part of the OVIDE track (from 41.4°W to 34°W) shown in Figure 1a. Contour lines show the silicate concentration (µmol $kg^{-1}$). ODV gridding interpolation (Schlitzer, 2002).

Fig. 8: $\Delta DIC^{eMLR}$ (Anthropogenic $CO_2$ change, µmol $kg^{-1}$) versus $\Delta\delta^{13}C_{DIC}{}^{eMLR}$ (oceanic $^{13}C$ Suess Effect, ‰) calculated from the extended Multi Linear Regression method between 1981 and 2006 in the Irminger Basin along the transect between 41.4°W and 34°W (Fig. 1a). The blue crosses symbolize the Denmark Strait Overflow Water (DSOW), the yellow circles show the North East Atlantic Deep Water (NEADW), the red triangles point out the Labrador Sea Water (LSWs) and the black dots indicate the subsurface water. Black line displays the theoretical $C_{ant}$ change estimated from the change in $\delta^{13}C_{DIC}$ by assuming a ratio of -0.015 ‰ (0.72 µmol $kg^{-1}$)$^{-1}$ $yr^{-1}$.

**Figure(s)**

**Click here to download Figure(s): fig1.pdf**

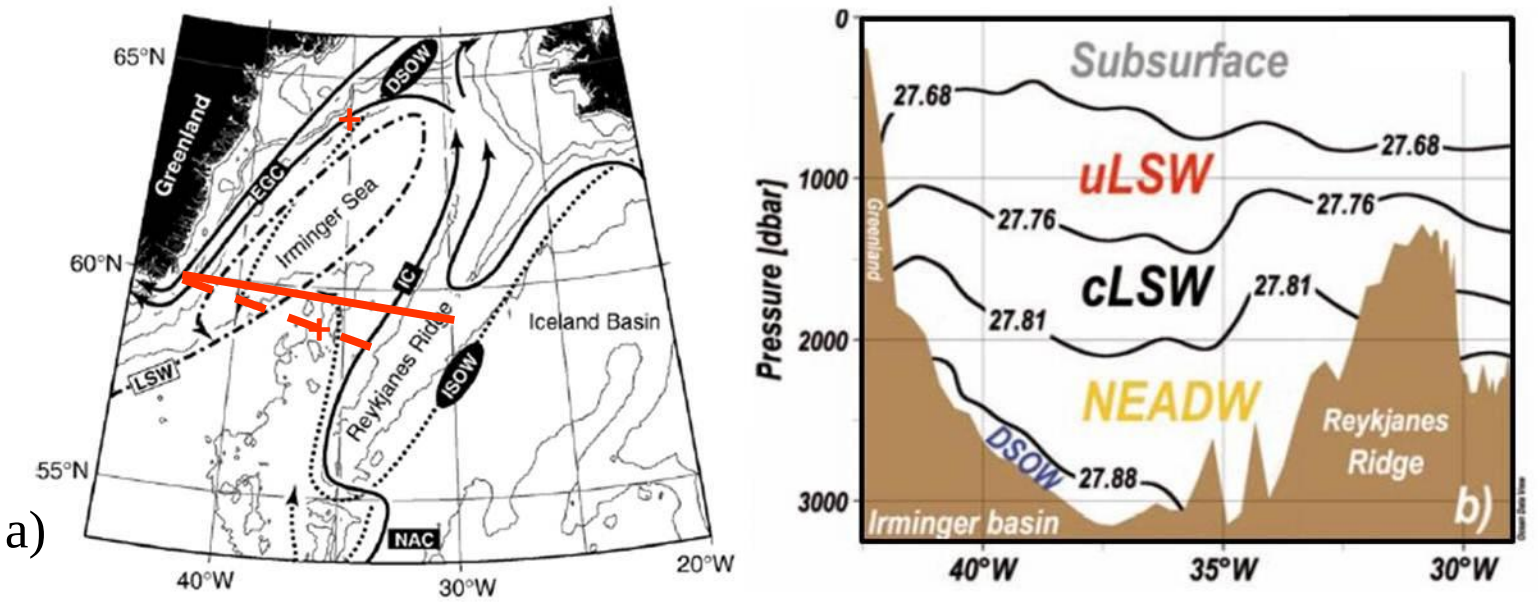


Fig. 1: Pattern of the main a) circulation (Holliday et al. 2006) and b) water masses (Perez et al., 2008) present in the Irminger Basin. The sea surface circulation is given by solid lines (NAC for North Atlantic Current, IC for Irminger Current and EGC for East Greenland Current). The mid-depth circulation is given by dot-dashed line (u/cLSW for upper/classical Labrador Sea Water). The deep circulation is given by dotted lines (ISOW for Iceland–Scotland Overflow Water which is modified by mixing with the LSW to formed NEADW, North East Atlantic deep water, and DSOW for Denmark Strait Overflow Water). The density ($\sigma\theta$) boundaries were established following Kieke et al. (2007) and Yashayaev et al. (2008). The Sampling locations in the Irminger Basin were shown by orange forms : the OVIDE samples (2002 and 2006) are given by the orange full line whereas the TTO samples (1981) are given by the orange dashed line. The crosses show both stations where $\delta^{13}C_{DIC}$ was collected during the TTO cruises while the OVIDE $\delta^{13}C_{DIC}$ measurements were regularly sampled in water column along OVIDE transect.

Figure(s)

Click here to download Figure(s): fig2.pdf

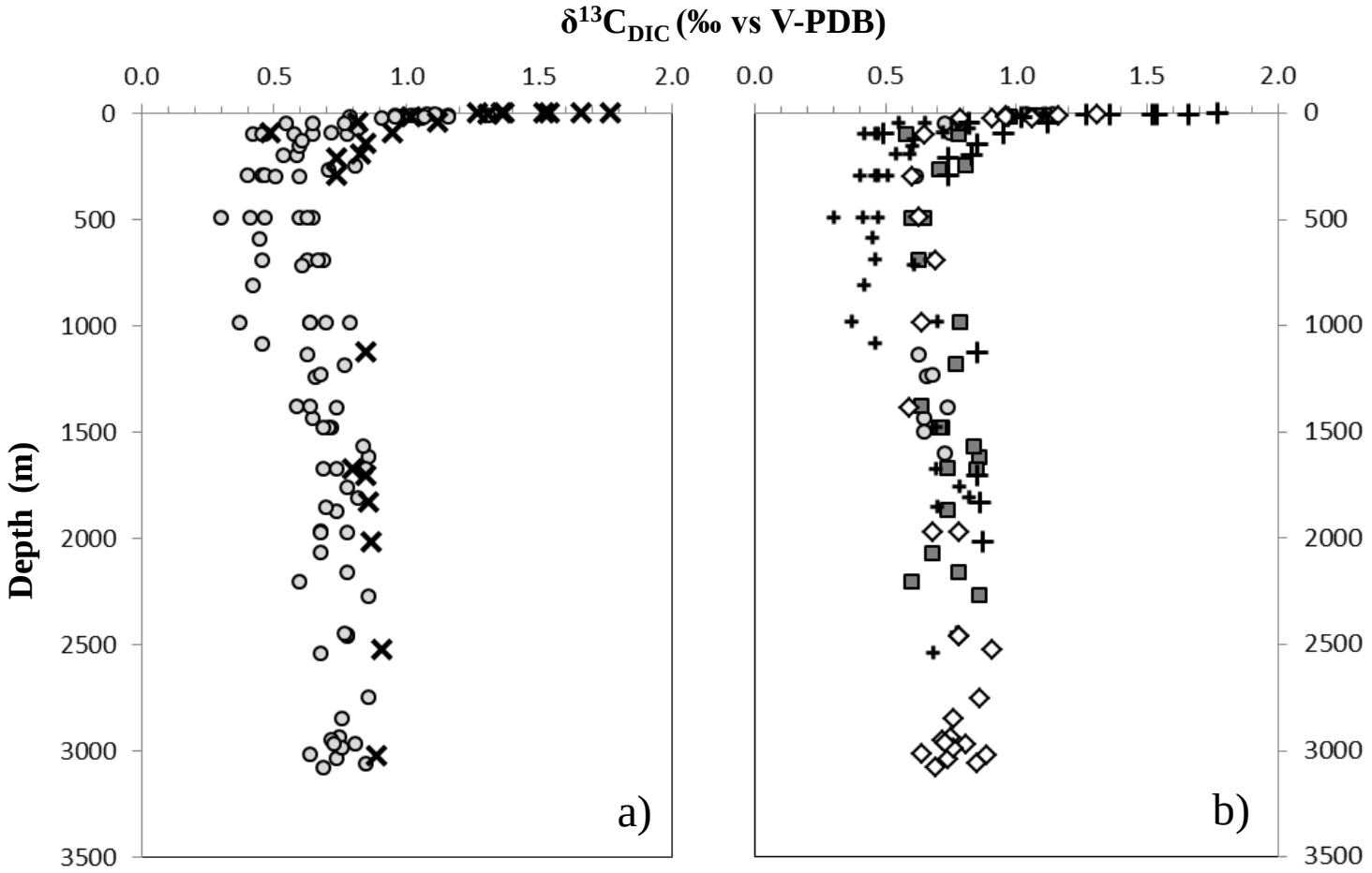


Fig.2: Vertical distribution of $\delta^{13}C_{DIC}$ (‰ vs V-PDB) sampled between the East Greenland Coast and 30°W a) during OVIDE cruises in 2002 (black crosses) and 2006 (grey circles). b) 4 area are distinguished according to the literature (Väge et al., 2005; Holliday et al., 2006): the zone of Reykanes ridges (light grey circles), the zone of the Irminger Current (dark grey squares), the Center of the Irminger Sea (open diamonds) and the Western Boundaries Current region (dark crosses)

Figure(s)

Click here to download Figure(s): fig3.pdf

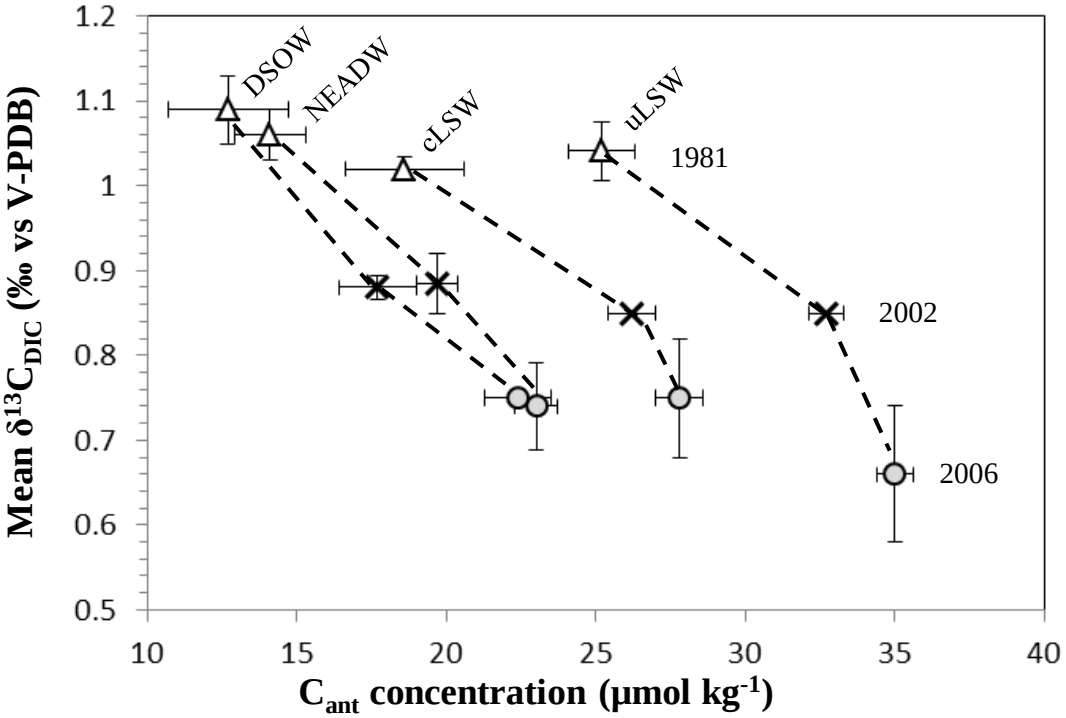


Fig.3 : Mean $\delta^{13}C_{DIC}$ (‰ vs V-PDB) versus mean anthropogenic carbon ($C_{ant}$) concentration (µmol $kg^{-1}$) estimated by Perez et al. (2010) with $\varphi C_T$ method for 1981 (open triangles), 2002 (black crosses) and 2006 (grey circles) for each water mass (dashed lines; from right to left, upper Labrador Sea Water (uLSW), classical Labrador Sea Water (cLSW), North East Atlantic Deep Water (NEADW) and Denmark strait Overflow Water (DSOW)). Each value is fitted with its standard deviation.

**Figure(s)**

**Click here to download Figure(s): fig4.pdf**

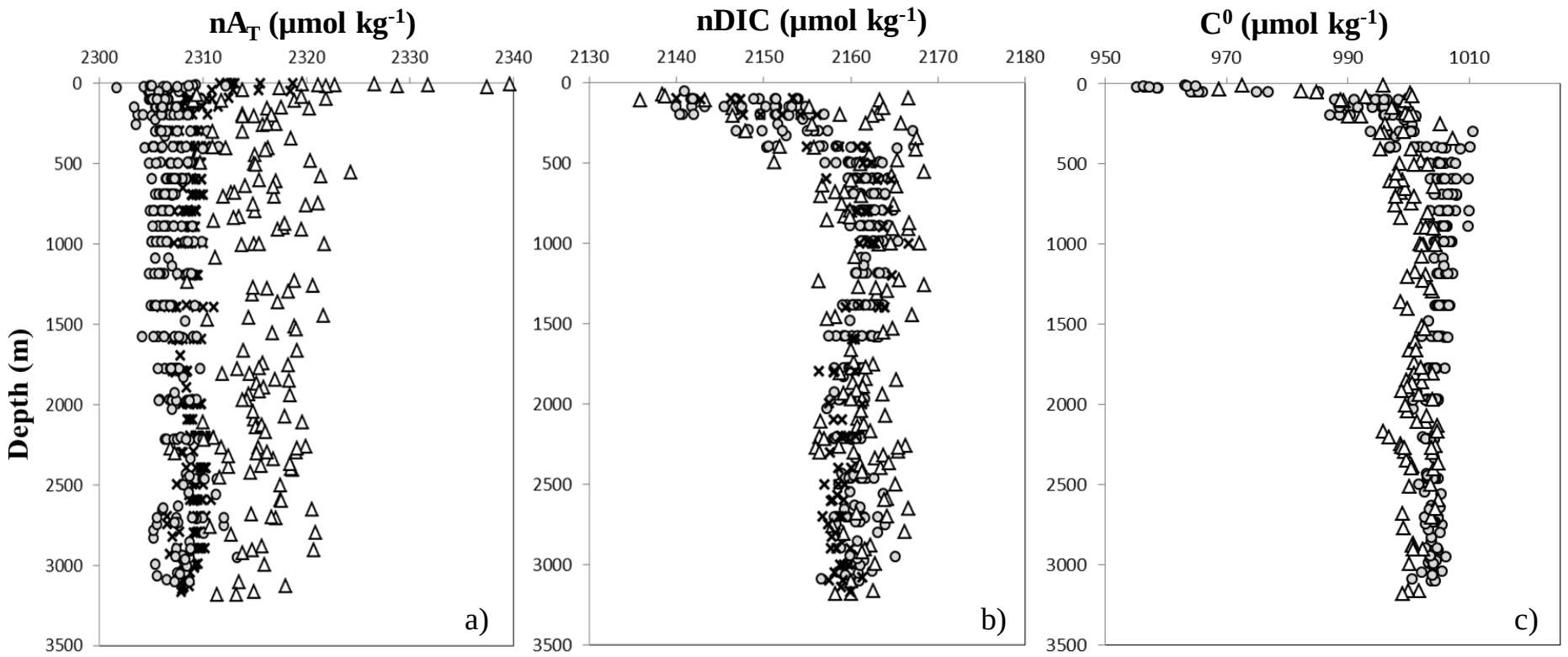


Fig.4: the vertical distribution of a) normalized Alkalinity by salinity ($nA_T$, µmol kg$^{-1}$), b) normalized Dissolved Inorganic Carbon (nDIC, µmol kg$^{-1}$) and c) preformed carbon ($C^0$ = DIC-0.5x$A_T$, µmol kg$^{-1}$) sampled during TTO-NAS 1981 (open triangle), OVIDE 2002 (black crosses) and OVIDE 2006 (grey circles).

Figure(s)

Click here to download Figure(s): Fig5.pdf

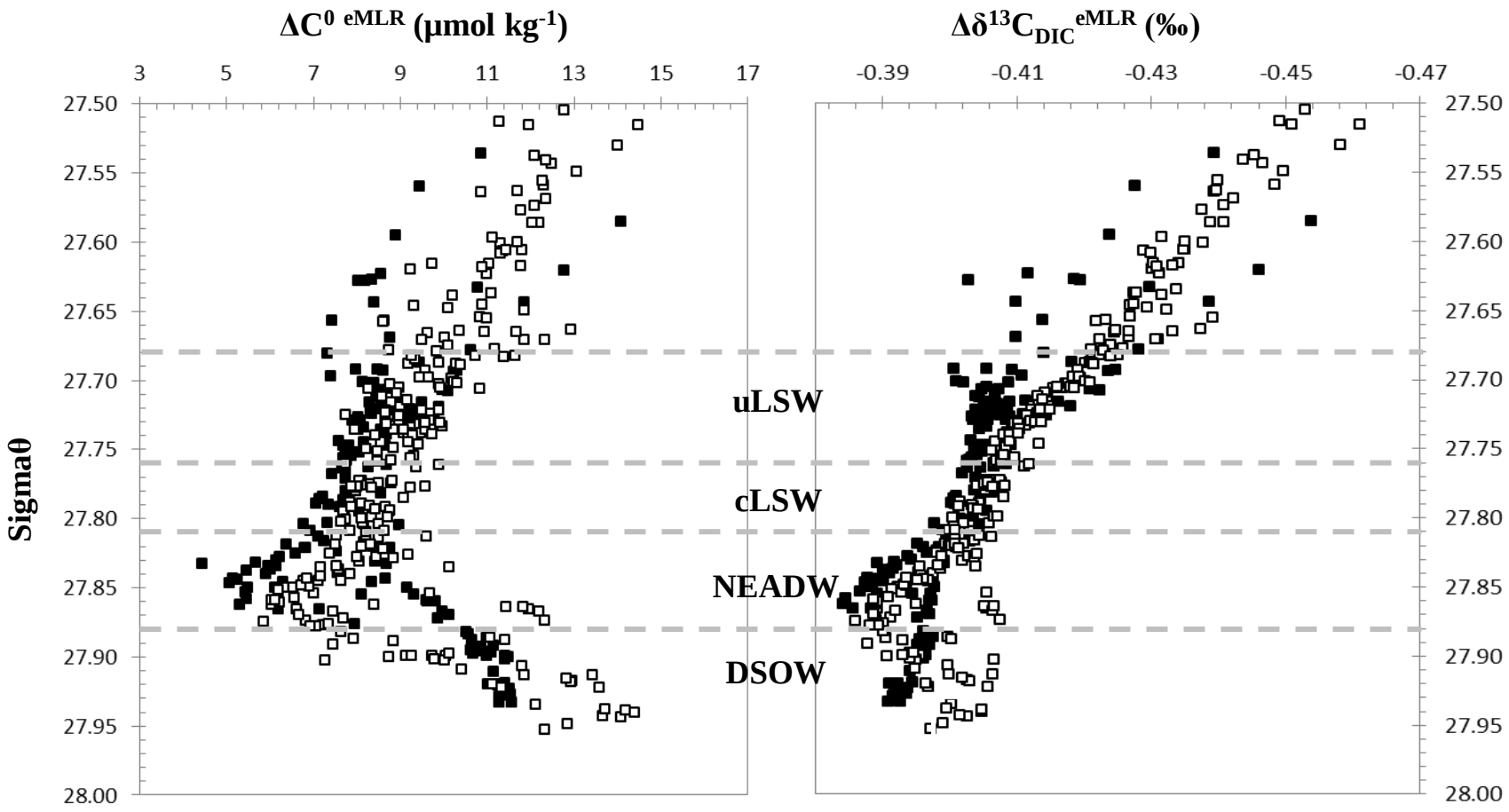


Fig.5 : Vertical distribution of $\Delta C^{0\ eMLR}$ and $\Delta\delta^{13}C_{DIC}{}^{eMLR}$ in function of sigma0. $\Delta C^{0\ eMLR}$ and $\Delta\delta^{13}C_{DIC}{}^{eMLR}$ are respectively calculated from fits #3 – #1 and fits #4 – #2 applied either on TTO data set (black squares) or on OVIDE 2006 data set (open squares). Greys dashed lines show water masses boundaries established following Kieke et al. (2007) and Yashayaev et al. (2008). u/cLSW: upper/classical Labrador Sea Water; NEADW: North East Atlantic Deep Water; DSOW: Denmark Strait Overflow Water.

Figure(s)

Click here to download Figure(s): FIG6.pdf

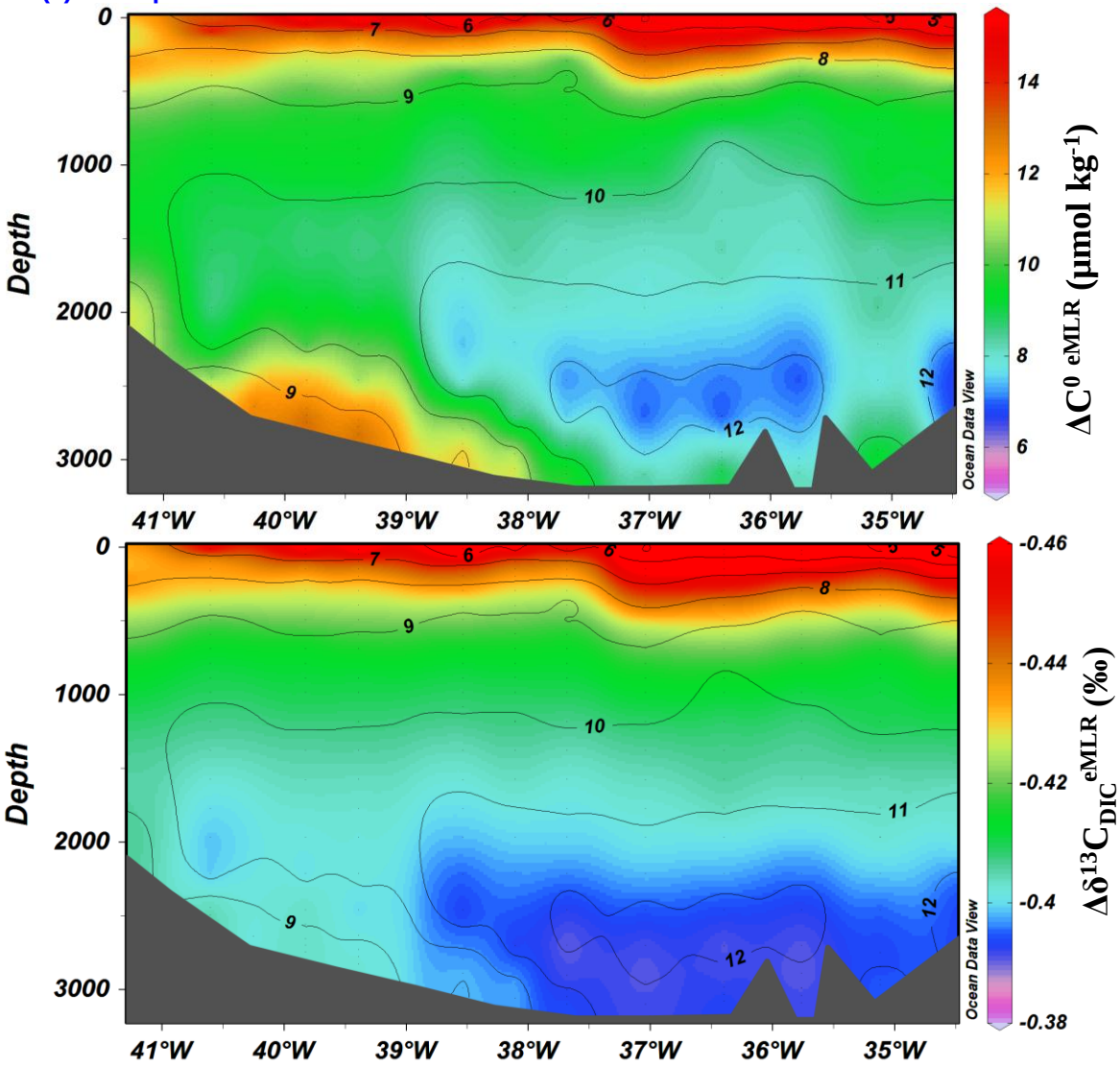


Fig.6: Estimated anthropogenic $\delta^{13}C_{DIC}$ decrease ($\Delta\delta^{13}C_{DIC}{}^{eMLR}$, ‰) and $CO_2$ increase ($\Delta C^{0\ eMLR}$, µmol kg$^{-1}$), in the Irminger Basin from 1981 to 2006, along a part of the OVIDE track (from 41.5°W to 34°W) shown in Figure 1a. Contour lines show the silicate concentration (µmol kg$^{-1}$ ). ODV gridding interpolation, Schlitzer, 2002

Figure(s)

Click here to download Figure(s): fig7.pdf

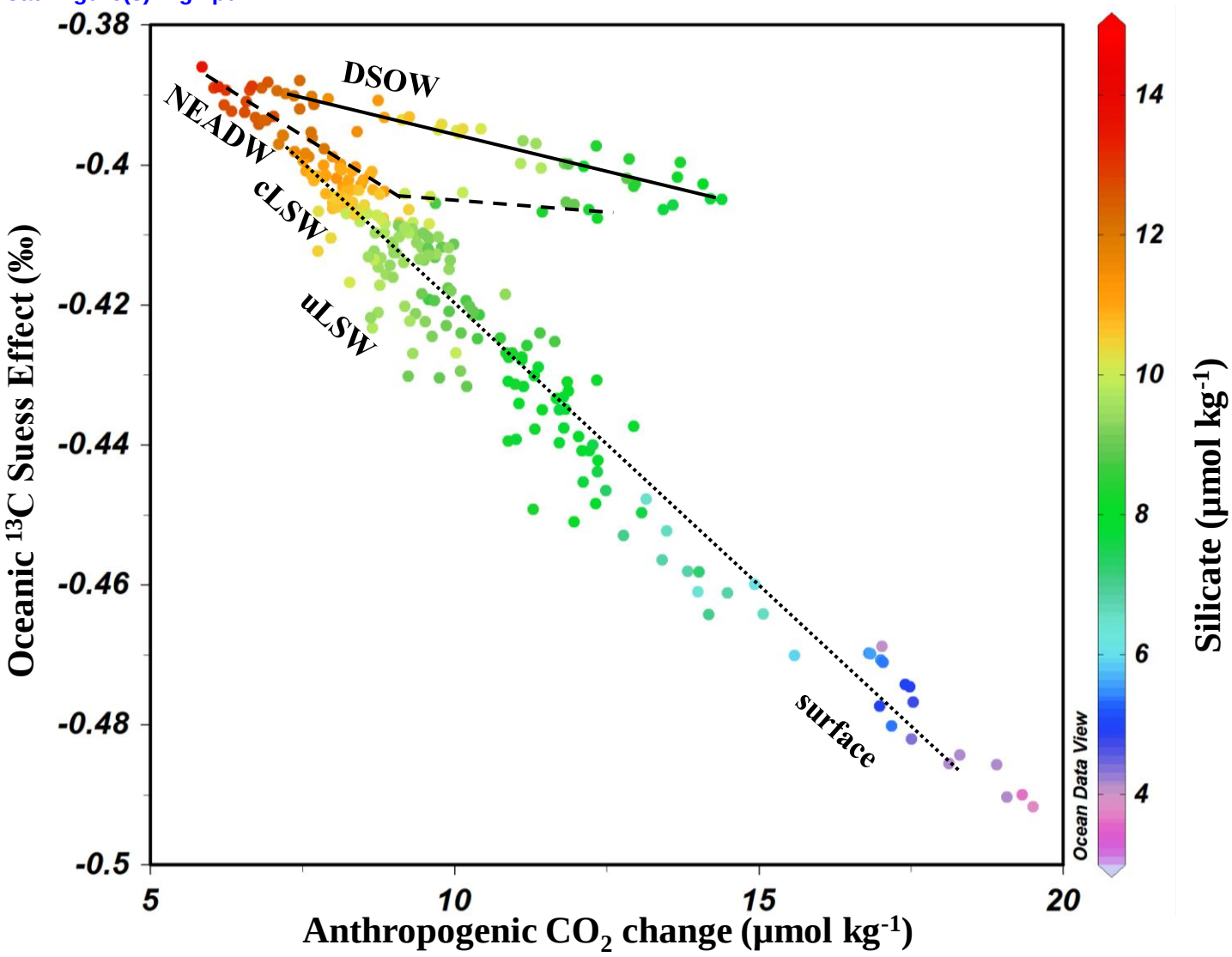


Fig.7: $\Delta\delta^{13}C_{DIC}{}^{eMLR}$ (Oceanic $^{13}$C Suess effect, ‰) versus $\Delta C^{0\ eMLR}$ (Anthropogenic $CO_2$ change, µmol kg$^{-1}$) and the silicate concentration (µmol kg$^{-1}$). The black line symbolize the Denmark Strait Overflow Water (DSOW), the black dashed line show the North East Atlantic Deep Water (NEADW) and the black dotted line point out the classical Labrador Sea Water (cLSW), the upper LSW and the surface.

**Figure(s)**

**Click here to download Figure(s): FigA1.pdf**

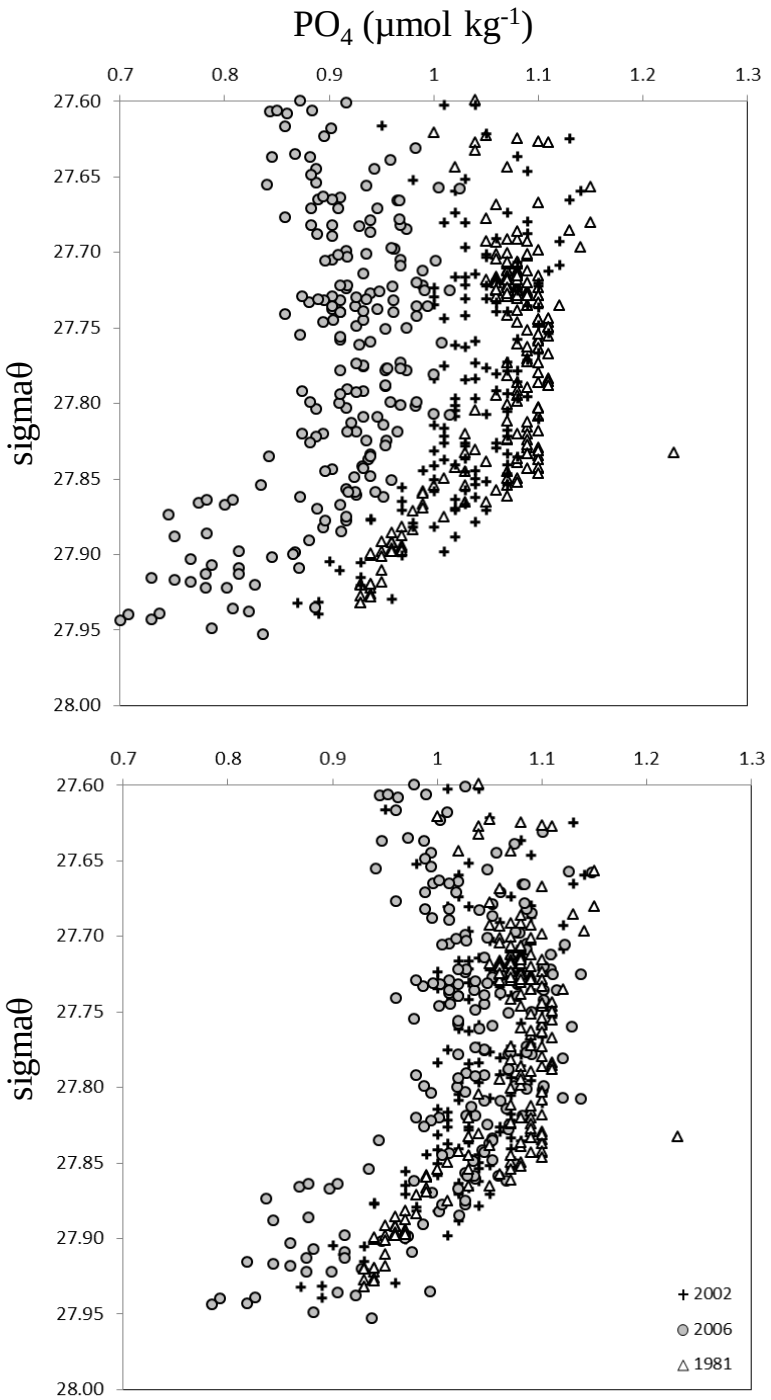


Fig.A1: Vertical distribution of Phosphate concentration ($PO_4$, µmol $kg^{-1}$) sampled between 41.4°W and 34°W in longitude and between 60°N and 59°N in latitude during TTO-NAS cruise in 1981 (open triangles) and during two OVIDE cruises in 2002 (black crosses) and in 2006 (grey circles).